10934 *Biochemistry* **2009,** *48,* 10934–10947
DOI: 10.1021/bi901570k

BIOCHEMISTRY
including biophysical chemistry & molecular biology
*Article*

# Denaturant-Dependent Conformational Changes in a β-Trefoil Protein: Global and Residue-Specific Aspects of an Equilibrium Denaturation Process

Ramil F. Latypov,*[,‡,@] Dingjiang Liu,[§,@] Jaby Jacob,[‡] Timothy S. Harvey,[∥] Pavel V. Bondarenko,[⊥] Gerd R. Kleemann,[‡] David N. Brems,[⊥] and Andrei A. Raibekas[⊥]

[‡]*Department of Analytical and Formulation Sciences, Amgen Inc., Seattle, Washington 98119,* [§]*Department of Analytical and Formulation Sciences, Amgen Inc., Thousand Oaks, California 91320,* [∥]*Department of Protein Science, Amgen Inc., Thousand Oaks, California 91320, and* [⊥]*Department of Formulation and Analytical Resources, Amgen Inc., Thousand Oaks, California 91320*
[@]*These authors contributed equally to this work.*

*Received September 8, 2009; Revised Manuscript Received October 16, 2009*

ABSTRACT: Conformational properties of the folded and unfolded ensembles of human interleukin-1 receptor antagonist (IL-1ra) are strongly denaturant-dependent as evidenced by high-resolution two-dimensional nuclear magnetic resonance (NMR), limited proteolysis, and small-angle X-ray scattering (SAXS). The folded ensemble was characterized in detail in the presence of different urea concentrations by $^{1}H-^{15}N$ HSQC NMR. The β-trefoil fold characteristic of native IL-1ra was preserved until the unfolding transition region beginning at 4 M urea. At the same time, a subset of native resonances disappeared gradually starting at low denaturant concentrations, indicating noncooperative changes in the folded state. Additional evidence of structural perturbations came from the chemical shift analysis, nonuniform and bell-shaped peak intensity profiles, and limited proteolysis. In particular, the following nearby regions of the tertiary structure became progressively destabilized with increasing urea concentrations: the β-hairpin interface of trefoils 1 and 2 and the H2a−H2 helical region. These regions underwent small-scale perturbations within the native baseline region in the absence of populated molten globule-like states. Similar regions were affected by elevated temperatures known to induce irreversible aggregation of IL-1ra. Further evidence of structural transitions invoking near-native conformations came from an optical spectroscopy analysis of its single-tryptophan variant W17A. The increase in the radius of gyration was associated with a single equilibrium unfolding transition in the case of two different denaturants, urea and guanidine hydrochloride (GuHCl). However, the compactness of urea- and GuHCl-unfolded molecules was comparable only at high denaturant concentrations and deviated under less denaturing conditions. Our results identified the role of conformational flexibility in IL-1ra aggregation and shed light on the nature of structural transitions within the folded ensembles of other β-trefoil proteins, such as IL-1β and hFGF-1.

Understanding the interplay between protein folding and aggregation requires information about the structure, stability, and dynamics of the various conformational states accessible to a polypeptide chain. Human recombinant interleukin-1 receptor antagonist (IL-1ra)[1] is a β-trefoil protein that suppresses inflammatory and immune responses mediated by interleukin-1α (IL-1α) and interleukin-1β (IL-1β) (*1*). Irreversible aggregation of IL-1ra induced by elevated temperatures or low-molecular weight additives has been a topic of research over the past few years (*2*−*7*). However, structural preferences of the folded and denatured states of IL-1ra and the role of equilibrium intermediates in its aggregation process remained unclear. Because of a high degree of sequence and structure similarity (*8*, *9*), the folding and stability of IL-1ra resemble those of the well-studied IL-1β (*10*). Both proteins display the archetypal β-trefoil global fold (*11*) in which six β-strands form a β-barrel (β1, β4, β5, β8, β9, and β12) capped at one side by another six β-strands forming a triangular array of hairpins (β2−β3, β6−β7, and β10−β11 hairpins) (*9*, *12*). Other examples of β-trefoil proteins with known folding properties include acidic and basic fibroblast growth factors and hisactophilin (*13*−*16*). The tertiary structure of β-trefoil proteins exhibits a pseudo-3-fold symmetry and is characterized by the presence of three repeating units (trefoils) consisting of 40−50 amino acids. The trefoils are structurally interdependent regions numbered as trefoils 1, 2, and 3, starting from the N-terminus. Experimental and computational studies suggested that folding of β-trefoil proteins is initiated in turns and continues with the stabilization of trefoils (*16*, *17*). For example, the folding of hisactophilin requires the formation of medium- and long-range interactions in trefoils 2 and 3, whereas IL-1β folds through the ends-together route (begins with trefoils 1 and 3) or via backtracking involving transient folding and unfolding of trefoil 3 (*17*, *18*). Available reports also suggested

*To whom correspondence should be addressed. E-mail: rlatypov@amgen.com. Phone: (206) 265-8851. Fax: (206) 217-0346.

[1]Abbreviations: ANS, 8-anilinonaphthalene-1-sulfonic acid; CD, circular dichroism; DTT, dithiothreitol; FRET, fluorescence resonance energy transfer; GuHCl, guanidine hydrochloride; HA-HCl, hydroxylamine hydrochloride; HPLC, high-performance liquid chromatography; HSQC, heteronuclear single-quantum correlation; H−D exchange, hydrogen−deuterium exchange; IL-1ra, interleukin-1 receptor antagonist; MS, mass spectrometry; MS/MS, tandem mass spectrometry; NMR, nuclear magnetic resonance; PDB, Protein Data Bank; $R_g$, radius of gyration; SAXS, small-angle X-ray scattering; 2D, two-dimensional.

 Published on Web 10/19/2009 

that equilibrium unfolding of these proteins exhibits protein-specific deviations from a highly cooperative two-state mechanism. For example, hFGF-1 populates a nativelike intermediate during equilibrium GuHCl unfolding (*13*, *14*), whereas IL-1$\beta$ does not populate distinct equilibrium intermediates but exhibits conformational transitions within its structurally flexible native state ensemble (*19*). Both proteins undergo small-scale structural perturbations associated with increased H−D exchange rates under mildly denaturing conditions (*14*, *19*). To identify factors that determine such deviations from cooperative unfolding, conformational properties of $\beta$-trefoil proteins need to be thoroughly investigated. In addition, near-native protein conformations may be biologically relevant, and their characterization is important from the perspective of protein function.

We previously reported that IL-1ra also deviated from a highly cooperative equilibrium unfolding mechanism (*10*). While fluorescence- and CD-monitored denaturation transitions of IL-1ra were consistent with a two-state unfolding, high-resolution NMR revealed small-scale structural perturbations within its native baseline region (*10*). Also, H−D exchange rates of IL-1ra were sensitive to the presence of various excipients, suggesting an unusually flexible native state ensemble (*2*). The lack of information about the nature of underlying structural transitions called for a more detailed analysis of IL-1ra denaturation.

In this study, we investigated equilibrium unfolding of IL-1ra using SAXS, high-resolution 2D NMR, and limited proteolysis. By comparing data generated by these highly informative and diverse techniques, we gained sufficient insight into the local and global characteristics of the protein in its different conformational states. Because of the growing interest in protein dynamics, particular attention was paid to the conformational behavior of IL-1ra within its native baseline region. As a result, we identified the location and scale of structural perturbations, which precede global unfolding of IL-1ra and potentially control its aggregation process.

## MATERIALS AND METHODS

High-purity recombinant human (nonglycosylated) IL-1ra was supplied by an Amgen manufacturing facility. The uniformly $^{13}C$- and $^{15}N$-labeled IL-1ra and its W17A mutant were produced as previously described (*10*). Urea and GuHCl were obtained from ICN Biomedicals, Inc. (Aurora, OH) (ultrapure grade). $^{1}H-^{15}N$ HSQC NMR measurements were performed on protein solutions containing 130 $\mu$M IL-1ra in 45 mM sodium phosphate buffer (pH 7.0) with 10% deuterium oxide ($D_2O$) and 5 mM DTT. SAXS, CD, and fluorescence measurements were performed on protein solutions containing 290, 25−60, and 10 $\mu$M IL-1ra, respectively, under identical conditions. In the case of urea denaturation, protein samples were supplemented with 8.8 mM HA-HCl to suppress carbamylation (*10*). All equilibrium denaturation experiments were performed at 25 °C; optical spectroscopy measurements were conducted as previously described (*10*).

*SAXS*. SAXS measurements were performed at the BioCAT ID-18 undulator beamline at the Advanced Photon Source (APS), Argonne National Laboratory (Argonne, IL). Scattering images were acquired using a Mar165 single-chip CCD area detector (MarUSA, Inc., Evaston, IL) with an exposure time of ~1 s. Sample solutions were passed through the 1 mm diameter capillary cell during equilibrium measurements. This procedure effectively reduced the exposure time of the sample to beam to 10 ms and helped avoid radiation damage. Blank scattering (identical conditions except without protein) was measured just before each measurement of the protein sample. The temperature was 25 °C for all measurements.

The SAXS data were analyzed using IGOR Pro (WaveMetrics, Inc., Lake Oswego, OR) macros written by the BioCAT staff at APS. $R_g$ and $I(0)$ were obtained on the basis of the Guinier approximation within the Guinier region ($R_gQ \leq 1.3$) (*20*, *21*):

$$\ln I(Q) = \ln I(0) - R_g^2 Q^2/3$$

*NMR Spectroscopy*. Urea denaturation experiments were performed at 25 °C using a Varian (Palo Alto, CA) INOVA 800 MHz NMR spectrometer equipped with a 5 mm triple-resonance probe.

$^{1}H-^{15}N$ HSQC spectra were acquired with 64 experiments conducted in the $^{15}N$ dimension ($t_1$) consisting of eight scans and 1024 data points in the $^{1}H$ dimension ($t_2$). The total experimental time for each spectral acquisition was 24 min. Spectra were processed using NMRPipe (*22*) and analyzed using NMRView (*23*). The $^{1}H-^{15}N$ cross-peak assignments from Stockman et al. (*24*) were used.

Temperature ramping experiments were performed using a Bruker (Billerica, MA) DRX Advance II 600 MHz NMR spectrometer equipped with an inverse TXI, *z*-gradient cryogenic probe, as previously described (*7*).

*Real-Time Proteinase K Digestion with Reversed-Phase HPLC−MS Analysis*. Broad specificity proteinase K (P5568, Sigma-Aldrich, St. Louis, MO) was used in the limited proteolysis experiments. Samples contained 60 $\mu$M IL-1ra in 50 mM sodium phosphate buffer (pH 7.0) with 3 mM DTT, 5 mM HA-HCl, and different levels of urea (0, 3, and 5 M). We made the first injection (see HPLC details below) immediately after mixing IL-1ra with the protease at an E:S ratio of 1:100. Samples were kept at 25 °C throughout the course of the experiment. Snapshots of the digestion process were obtained via repeated sample injections. The chromatograms were analyzed and integrated using Chemstation (Agilent, Palo Alto, CA).

Reversed-phase HPLC−MS analysis was performed on an Agilent 1100 Capillary HPLC system online with a Waters electrospray ionization (ESI) quadrupole time-of-flight (Q-TOF) Micro mass spectrometer according to the previously described protocol utilizing the buffer with 70% 2-propanol in solvent B (*25*). A 2 $\mu$g protein sample was injected on the Zorbax Stable Bond SB300 C8 50 mm × 1 mm column operated at 50 °C, and a linear gradient of B increasing from 30 to 45% was utilized for elution and separation of IL-1ra and its fragments. The column eluate was analyzed with the UV detector at 215 nm and then directed to an online mass spectrometer.

Identification of peptides produced by the limited proteolysis was performed by MS/MS analysis on a hybrid linear quadrupole ion trap [Orbitrap mass spectrometer (LTQ Orbitrap, Thermo Scientific, Bremen, Germany)] connected online to the Agilent 1100 Capillary HPLC system. The LTQ-Obritrap was opearated using the previously described method (*26*). A program developed at Amgen, MassAnalyzer, was used to automatically identify the digestion products by correlating the acquired fragmentation mass spectra to the sequence of IL-1ra.

## RESULTS

*SAXS-Detected Unfolding Equilibrium*. Equilibrium unfolding of IL-1ra was monitored by SAXS to measure its radius

of gyration ($R_g$) in the presence of different urea and GuHCl concentrations. Guinier plots [ln $I(Q)$ versus $Q^2$ plot (*20*)] of the scattering curves for the native protein at concentrations of 2, 5, and 7 mg/mL demonstrated an expected increase in zero-angle scattering intensity, $I(0)$, with an increasing protein concentration (data not shown) (*20*). The scattering curves showed no rollover in low $Q^2$ regions for any of the protein concentrations, indicating the absence of a strong interparticle interference effect (*20*, *27*) within this concentration range. Equilibrium unfolding experiments were conducted using 5 mg/mL (290 $\mu$M) protein solutions which provided high-quality data with no significant complications due to aggregation.

Panels A and B of Figure 1 show the Kratky plots [$I(Q)Q^2$ vs $Q$ plot] (*20*, *28*) of the scattering curves measured at various urea and GuHCl concentrations, respectively. At 0−4 M urea, a peak was observed at $Q \approx 0.1$ Å$^{-1}$ (see Figure 1A), indicating a compact globular structure of the protein. A striking change in the Kratky plots occurred only at higher denaturant concentrations and coincided with the unfolding transition region (see below). In the case of GuHCl, a similar peak was present up to ~1.1 M denaturant, but there was a slight change in its position and shape upon addition of as little as 0.4 M GuHCl (see Figure 1B). Besides this, no significant changes in the position of this peak were noticed either in urea or in GuHCl. Further increase in the denaturants resulted in Kratky profiles exhibiting a monotonic increase, which is expected for expanded coil-like chain conformations (*29*, *30*).

The $I(0)$ values decreased with increased denaturant levels in an approximately linear fashion, consistent with a decrease in the net electron density contrast between solute and solvent (*20*, *31*, *32*). There was a noticeable plateau coincident with the unfolding transition region for both denaturants that could be due to some low level of protein aggregation (data not shown).

The unfolding transition curves were monitored by $R_g^2$ which is a preferred way of analyzing SAXS denaturation data [$R_g^2$ is proportional to the scattering intensity and can be represented as a linear combination of the fractions of native and unfolded states (*33*)], and Figure 2A shows experimental results for both denaturants. Fitting of a two-state model to the $R_g^2$ data was done by assuming linear baselines for the folded and unfolded states, and the equilibrium parameters are listed in Table 1. The SAXS-based estimates of $\Delta G_{NU}$ were comparable between the denaturants, and the data agreed well with the results of the far-UV CD measurements (the normalized data are shown in Figure 2B). In accordance with the previous results (*2*), there was a large difference between the denaturing strength of urea versus GuHCl. Whereas GuHCl is generally 1.5−2.5 times more effective as a protein denaturant than urea (*34*), for IL-1ra the corresponding $C_m$ values (denaturation midpoints) varied ~3.5-fold. Together with notable differences in the folding and unfolding rates in urea and GuHCl (kinetic folding experiments by R. F. Latypov, unpublished data), this result suggested sensitivity of the IL-1ra structure to the ionic strength of the solvent.

A few representative Guinier plots that are shown in Figure 1C illustrate the dependence of the protein size on the GuHCl concentration. There was no significant change in the size of IL-1ra up to 1.1 M GuHCl, and its $R_g$ remained close to 17.36 ± 0.07 Å, which was somewhat smaller than the $R_g$ of the native apomyoglobin (a 154-residue protein) that varied from 18.2 Å (*35*) to 19.7 ± 1.3 Å (*21*). Our estimate of $R_g$ corroborated previously measured hydrodynamic diameter of IL-1ra

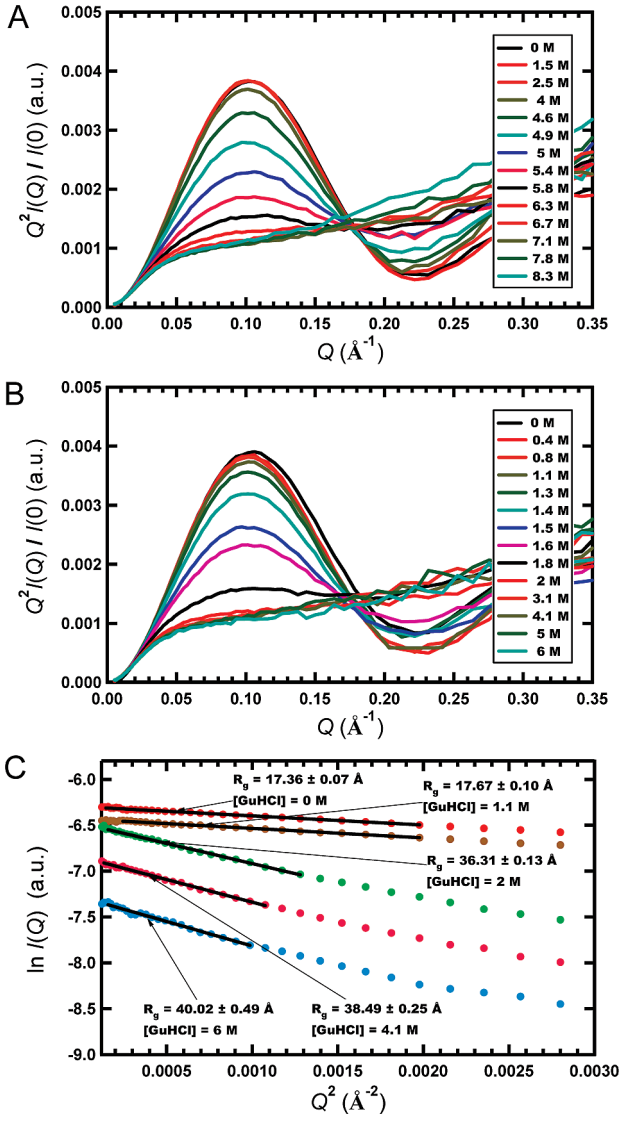


FIGURE 1: SAXS measurements. The Kratky plots of IL-1ra in the presence of various (A) urea and (B) GuHCl molar concentrations, as indicated. The scattering intensities are in arbitrary units. (C) Representative Guinier plots and estimated $R_g$ values for GuHCl-induced denaturation. To accurately measure the $R_g$, scattering data must be taken across angles where the Guinier approximation holds ($Q \leq 1.3/R_g$). Our reliable data start at $Q_{min}$ values of ~0.01 −0.02 Å$^{-1}$ (for $R_g$ = 41 Å, $Q_{max}$ = 0.032 Å). This low $Q_{min}$ value, along with the linearity in the Guinier plot, demonstrates that the $R_g$ can be reliably obtained from these data.

(3.4 ± 0.3 nm) using dynamic light scattering (*5*). As far as the unfolded conformation, its GuHCl dependence deviated from a horizontal line (Figure 2A) and could be extrapolated down to 35.4 ± 0.6 Å at 0 M denaturant. This estimate lies within the lower limit of values expected for random-coil chains consisting of 153 residues (34.2−44.5 Å; within a 95% confidence interval) (*30*). Figure 1C shows examples of the Guinier plots corresponding to 2−6 M GuHCl where an incremental change in the $R_g$ is observed (see also Figure 2A). Extrapolation of the $R_g$ for the urea-unfolded IL-1ra was not attempted due to a less defined post-transition baseline. However, we noted differences in the $R_g$ of denatured molecules at the completion of respective GuHCl- and urea-induced transitions, which disappeared only at higher denaturant concentrations (Figure 2A).

Figure 2B shows an overlay of the normalized unfolding curves measured by SAXS and far-UV CD. As follows from

the close correspondence of the data, both techniques detected the same conformational transition between the folded and unfolded states. The apparent two-state mechanism of protein denaturation was supported by the Kratky plots that showed an iso-scattering point at $Q \approx 0.18$ Å$^{-1}$ in the case of both denaturants (cf. Figure 1A,B). Overall, no evidence of any measurable accumulation of partially folded protein conformations was found.

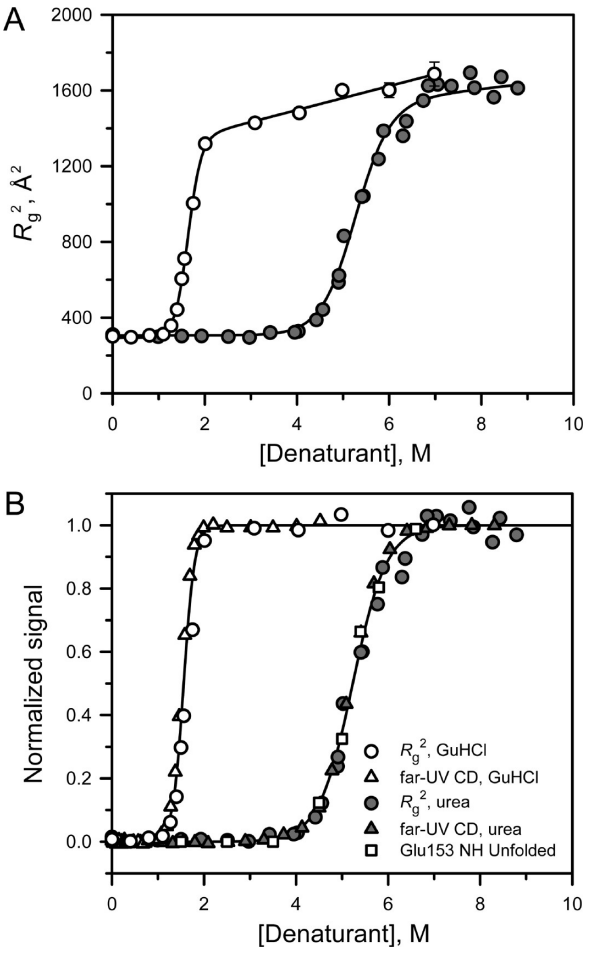


FIGURE 2: SAXS and CD measurements. (A) GuHCl- and urea-induced unfolding of IL-1ra as monitored by $R_g^2$ (○ and ●, respectively). Errors are standard errors of the Guinier fitting (in many cases, the error bars are smaller than the symbols). The solid lines represent the best fits to a two-state denaturation model. (B) Normalized GuHCl- and urea-induced unfolding transitions measured by SAXS (circles) and far-UV CD (triangles). The GuHCl and urea data are depicted as white and gray symbols, respectively. The squares illustrate changes in the normalized peak intensity for the unfolded state resonance of Glu153 [available for urea denaturation only (see text)].

*NMR-Detected Unfolding Equilibrium.* (*i*) *Urea-Dependent Chemical Shift Changes*. Our earlier NMR measurements revealed nonuniform peak intensity variations under subdenaturing conditions (*10*), which required more detailed investigation. In this study, we acquired a series of $^1$H−$^{15}$N HSQC spectra of a uniformly $^{13}$C- and $^{15}$N-labeled IL-1ra preincubated with different concentrations of urea (see Figure S1 of the Supporting Information). Because of slow conformational exchange (*10*), it was possible to monitor resonances from the folded and denatured states of the protein within a wide range of conditions. Because of partial peak overlap and missing assignments [primarily from the N-terminal part of the protein (*24*)], only 88 native resonances were analyzed in terms of their chemical shifts and intensity. Both amide proton and amide nitrogen chemical shifts were used as reporters of structural changes, and panels A and B of Figure 3 illustrate changes induced by 3.5 M urea. It can be seen that addition of denaturant caused structural perturbations along the entire length of the protein. The overall chemical shift change continuously increased throughout the pretransition region. The majority (~60%) of the folded state peaks exhibited linear $^1$H chemical shift dependencies up until the unfolding region (illustrated by the amide peak of Asp75 in Figure S2 of the Supporting Information). The most pronounced chemical shift change was exhibited by the cross-peak of Leu31 (Figure 3A,B), which was previously shown to be induced by urea binding (*10*). Many of its neighboring residues (Thr23, Leu26, Arg27, Gln30, Val32, Gly34, and Tyr35) also exhibited chemical shift variations that were consistent with urea binding (illustrated by the amide peak of Arg27 in Figure S2). Taken together, the data pinpointed at the $\beta2-\beta3$ hairpin from the hairpin cap, and a similar trend was observed for the other two hairpins ($\beta6-\beta7$ and $\beta10-\beta11$). Specifically, we identified the following positions within the $\beta6-\beta7$ and $\beta10-\beta11$ hairpins and their flanking regions: Leu59, Lys65, Cys67, Cys70, Arg78, Glu82, Ala83, Asn85, Leu89, Phe101, Ile102, Ser114, Ala115, Cys117, Asp129, Gln130, and Val132. This susceptibility to urea binding distinguished the hairpin cap from the $\beta$-barrel, where linear $^1$H chemical shift dependencies were more common. Another interesting observation was the similarity of $^1$H chemical shift changes for Ala33 and Ala125 (Figure S2). Although these residues belong to different hairpins ($\beta2-\beta3$ and $\beta10-\beta11$ hairpins, respectively) and trefoils (1 and 3, respectively), they are proximal to each other in the folded protein. Their strikingly similar chemical shift profiles were indicative of changes in the tertiary structure of the protein under conditions where accumulation of the unfolded state was negligible.

Table 1: Thermodynamic Parameters of IL-1ra Obtained by Fitting of a Two-State Model to the Urea- and GuHCl-Induced Unfolding Transitions at 25 °C

| biophysical method | denaturant | $C_m$ (M) | $m$ (kcal mol$^{-1}$ M$^{-1}$) | $\Delta G_{NU}$ (kcal mol$^{-1}$) |
|---|---|---|---|---|
| SAXS | GuHCl | 1.59 ± 0.02 | 5.69 ± 0.94 | 9.1 ± 1.6 |
| far-UV CD | GuHCl | 1.51 ± 0.01 | 5.39 ± 0.10 | 8.1 ± 0.2 |
| SAXS | urea | 5.25 ± 0.06 | 1.59 ± 0.20 | 8.3 ± 1.2 |
| far-UV CD | urea | 5.21 ± 0.01 | 1.76 ± 0.03 | 9.2 ± 0.2 |
| | | 5.19 ± 0.03[a] | 1.09 ± 0.05[a] | 5.7 ± 0.3[a] |
| NMR | urea | 5.24 ± 0.12[b] | 1.04 ± 0.15[b] | 5.5 ± 0.9[b] |
| | | 5.21 ± 0.17[c] | 1.66 ± 0.30[c] | 8.7 ± 1.8[c] |

[a]Average thermodynamic parameters of IL-1ra based on 48 native amide resonances exhibiting cooperative unfolding (see the text). [b]Residue-specific equilibrium unfolding parameters for the native state resonance of Glu153 (see the text). [c]Residue-specific equilibrium unfolding parameters for the unfolded state resonance of Glu153 (see the text).

Although addition of urea induced widespread structural perturbations, some regions of the protein exhibited much greater changes in the electronic and electrostatic environment than others. This was especially apparent from the $^{15}N$ chemical shift data which showed clustered perturbations roughly centered at the 30th, 80th, and 130th residue positions, approximately 50 residues apart (Figure 3B). Specifically, perturbations at positions 23−34 coincided with the entire $\beta2-\beta3$ hairpin that contained residues implicated in urea binding (see above). Another two regions coincided with the $\beta6-\beta7$ and $\beta10-\beta11$ hairpins: note, in particular, residues Lys72, Gln80, Ala83, Val84, and Ser133. The only significantly shifting cross-peak outside of the hairpin triplet corresponded to Ile47. Thus, the profile of the $^{15}N$ chemical shift perturbations was clearly identifiable with the $\beta$-hairpins of the hairpin cap. In contrast, it was more difficult to interpret the $^{1}H$ chemical shifts (Figure 3A): besides Leu31, only five residue positions exhibited chemical shift perturbations exceeding 0.1 ppm prior to unfolding (Arg27, Cys67, Phe101, Glu140, and Thr145), suggesting that IL-1ra remained in a largely folded conformation.

(*ii*) *Urea-Dependent Peak Intensity Variations*. A characteristic feature of IL-1ra denaturation is the nonuniformity of peak intensity variations exhibited by its native resonances (see Figure S3 of the Supporting Information). Figure 4A illustrates normalized peak intensity changes exhibited by a few representative peaks. In many cases, the disappearance of the native state resonances coincided with global unfolding. Although residue-specific denaturation profiles varied significantly, negatively sloped pretransition baselines were the most abundant, and ~70% of the profiles were similar to those of Gln12 (gray triangles) and Gln130 (black triangles). Forty-eight resonances provided high-quality denaturation data for global curve fitting analysis based on a two-state model. The estimated equilibrium parameters are listed in Table 1, and the average fit is shown in

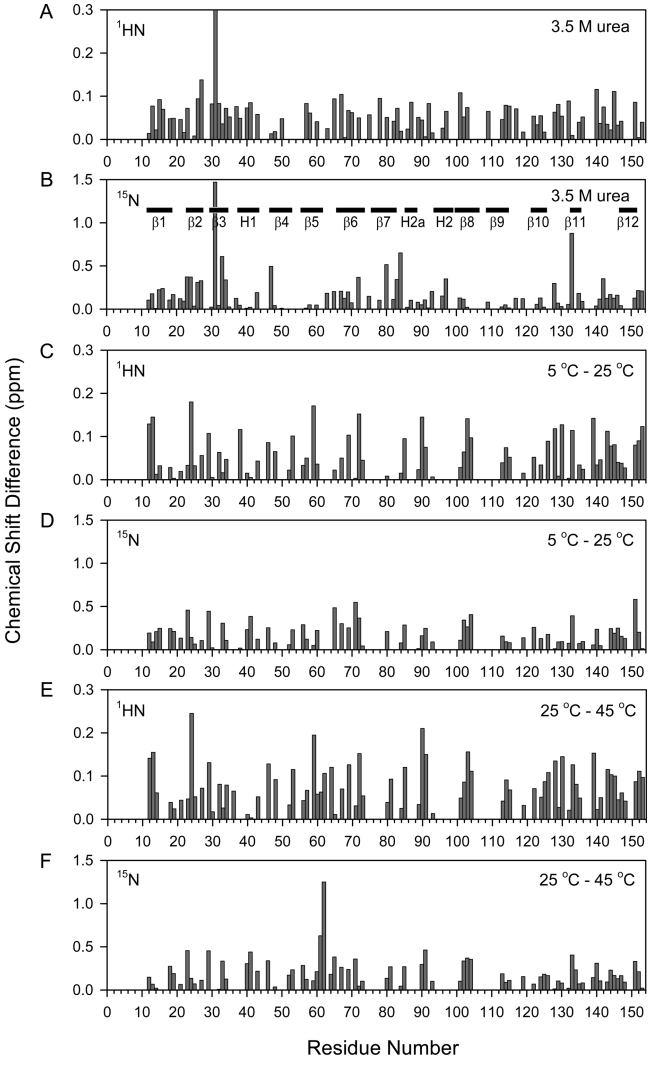


FIGURE 3: Chemical shift changes among native $^{1}HN$ and $^{15}N$ resonances of $^{13}C$- and $^{15}N$-labeled IL-1ra. The graphs show residue-specific perturbations induced by 3.5 M urea (A and B), a temperature change from 5 to 25 °C (C and D), and a temperature change from 25 to 45 °C (E and F). For every condition, the $^{1}HN$ and $^{15}N$ chemical shifts are plotted separately as they provide a different type of structural information (see the text). For ease of comparison, the chemical shift differences are shown as absolute numbers. The largest chemical shift perturbation exhibited by Leu31 was previously attributed to a site-specific binding of urea (*10*). The location of the 12 $\beta$-strands and the three $3_{10}$-helices is indicated in panel B (*9*).

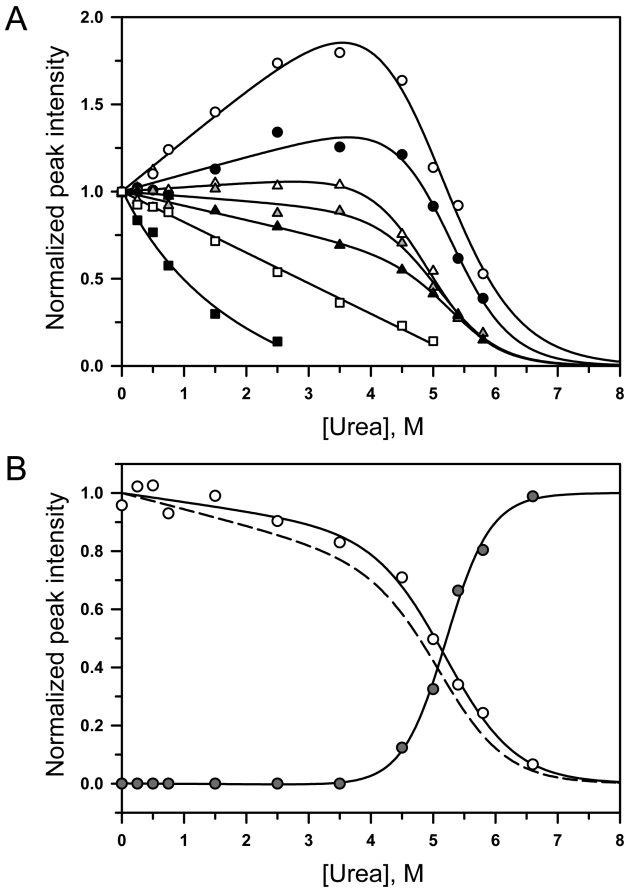


FIGURE 4: Residue-specific peak intensity variations as a function of urea concentration. (A) Denaturant-dependent changes for a representative set of native amide peaks. The peak intensities were normalized with respect to the 0 M urea spectrum. Residues and symbols (top to bottom): Gly38 (white circles), Asp75 (black circles), Asn92 (white triangles), Gln12 (gray triangles), Gln130 (black triangles), Glu82 (white squares), and Asn85 (black squares). Solid lines in the case of Gly38, Asp75, Asn92, Gln12, and Gln130 represent the best fits of a two-state denaturation model to the normalized data. Solid lines in the case of Glu82 and Asn85 are model-independent and shown for illustrative purposes only. (B) Normalized peak intensity variations for a pair of amide resonances of Glu153 originating from the folded and unfolded states (*7*) (shown by the white and gray symbols, respectively). Solid lines represent the best fits of a two-state denaturation model to their normalized intensity, whereas the dashed line shows the average two-state fit for a total of 48 native resonances (see the text).

Figure 4B (dashed line). The average midpoint ($C_m$) for the NMR-detected denaturation was close to that obtained from optical spectroscopy measurements (*10*), whereas the *m* value was considerably lower. As a result, $\Delta G_{NU}$ of the protein as determined by NMR appeared to be substantially lower (Table 1). This aspect was examined further by using a pair of Glu153 resonances originating from the folded and unfolded states of IL-1ra (*7*). Since Glu153 is the C-terminal residue that does not exhibit substantial conformational exchange (NMR relaxation experiments by T. S. Harvey and D. Liu, unpublished results), this pair of resonances served as a useful probe of protein denaturation. Figure 4B shows normalized peak intensity variations of these two resonances together with the corresponding two-state fits. In Figure 2B, the normalized peak intensity for the unfolded state resonance is overlaid with the SAXS and CD data (see the white squares). The equilibrium parameters for the native peak were very close to the average NMR values and corresponded to the lower estimate of $\Delta G_{NU}$, whereas results for the unfolded peak were virtually indistinguishable from those of SAXS and far-UV CD measurements (Table 1). This suggested that the discrepancy in the *m* values was related to the loss of the native peak intensity associated with the negatively sloped pretransition baselines, likely because of a growing population of another conformational state.

As illustrated by Gly38 and Asp75 in Figure 4A, some of the native resonances exhibited positively sloped pretransition baselines. Their peak intensities increased in an apparently linear fashion and reached the maximum by the unfolding transition region. At present, such behavior is known to be limited to the peaks of Gly38 and Asp75 that approached normalized values of ~1.7 and ~1.3, respectively, by 4 M urea.

Another group of residues exhibited nonsigmoidal peak intensity variations indicative of noncooperative changes in the protein structure. Their denaturation profiles were similar to those of Glu82 and Asn85 in Figure 4A as they showed little or no evidence for the unfolding process between 4 and 6 M urea. The majority of these residues lost a significant portion (> 50%) of their native intensity prior to unfolding and was distributed within the $\beta$-trefoil structure in a nonrandom way. With the exception of Ala125 and Lys146, the rest of the residues [18 of 20 residues total (see Table 2)] formed a large and well-defined cluster (see Figures 7A and 8A,B). This cluster was formed exclusively by the residues from trefoils 1 [residues 1−52 (*9*)] and 2 [residues 53−106 (*9*)]: Ile16, Phe24, Leu31, Ile47, Asp48, Leu59, Gly60, Gly63, Gly64, Lys65, Cys67, Leu68, Ser69, Glu82, Val84, Asn85, Ile86, and Ala100. These positions resided within the $\beta$1, $\beta$4, and $\beta$5 strands, the $\beta$2−$\beta$3 and $\beta$6−$\beta$7 hairpins, and the $3_{10}$ H2a−H2 helices [residues 86−88 and 94−99 (*9*)]. As for Ala125 and Lys146 from trefoil 3 [residues 107−153 (*9*)], they belong to the hairpin cap (specifically, to the $\beta$10−$\beta$11 hairpin), but their clustering is less evident. Overall, a large number of noncooperatively unfolding positions was associated with a contiguous area of the protein structure susceptible to structural and dynamic changes under moderately denaturing conditions.

(*iii*) *Minor Peaks*. High-quality data acquired in this study allowed detection of some minor resonances that showed distinct behavior from the peaks originating from the native and unfolded states. Figure 5 shows two unassigned minor peaks from two different regions of the $^1H-^{15}N$ HSQC spectra as a function of urea concentration. These peaks were absent under native conditions (~0 M urea) but gained intensity as the denaturant concentration increased. The intensity of one of these peaks increased continuously from ~1.5 M urea up to the unfolding transition region (see Figure 5A). A further increase in the level of urea led to its disappearance which coincided with global unfolding of the protein. Qualitatively similar behavior was exhibited by another minor peak shown in Figure 5B. The intensity of this peak changed very differently from that of the neighboring amide resonance of Phe147. The intensity of native Phe147 continuously decreased as a function of urea, whereas the minor peak steadily grew. At some point, intensities of these two peaks became equal (within the unfolding transition region) prior to their complete disappearance above 6 M urea. Although no resonance assignments are currently available for any of the minor peaks, their bell-shaped denaturant dependencies are clear indications of noncooperative changes in the protein structure. In some cases, these peaks were seen in the proximity of resolved native peaks, suggesting accumulation of nativelike conformations in slow exchange with the native state (Figure 5B).

Table 2: Structural Location of IL-1ra Residues Exhibiting Rapid or Noncooperative Loss of Native $^1H-^{15}N$ HSQC Peak Intensity in Urea

| residue | secondary structure[a] | $\beta$-trefoil[a] |
|---|---|---|
| Ile16 | $\beta$1 strand | 1 |
| Phe24 | $\beta$2 strand | 1 |
| Leu31 | $\beta$3 strand | 1 |
| Ile47 | $\beta$4 strand | 1 |
| Asp48 | $\beta$4 strand | 1 |
| Leu59 | $\beta$5 strand | 2 |
| Gly60 | $\beta$5 strand | 2 |
| Gly63 | loop region | 2 |
| Gly64 | loop region | 2 |
| Lys65 | loop region | 2 |
| Cys67 | $\beta$6 strand | 2 |
| Leu68 | $\beta$6 strand | 2 |
| Ser69 | $\beta$6 strand | 2 |
| Glu82 | $\beta$7 strand | 2 |
| Val84 | loop region | 2 |
| Asn85 | loop region | 2 |
| Ile86 | H2a $3_{10}$ helix | 2 |
| Ala100 | $\beta$8 strand | 2 |
| Ala125 | $\beta$10 strand | 3 |
| Lys146 | loop region | 3 |

[a]Based on the crystal structure of IL-1ra (*9*).

*Limited Proteolysis*. Limited proteolysis can serve as an alternative technique for detecting subtle conformational changes in proteins (*14*, *36*). To measure the structural flexibility of IL-1ra, proteinase K digestion experiments were performed on protein samples containing 0, 3, and 5 M urea. Proteinase K has broad specificity toward aliphatic and aromatic amino acids and can be used to assess multiple sites on proteins. The time-dependent proteolysis was monitored by real-time reversed-phase HPLC−mass spectrometry analysis (see Materials and Methods). The high column temperature and the low pH of the mobile phase ensured on-column dissociation of digested protein molecules into peptides. Consistent with our previous results (*3*), the first detectable event was truncation of the disordered N-terminal segment. Subsequently, the protein was cleaved at multiple positions generally similar between 0 and 3 M urea (see Figure S4 of the Supporting Information). Identification of flexible regions was achieved by taking snapshots of the kinetic digestion process followed by peptide identification and peak integration. In the absence of urea, the protein was resistant to proteolysis and contained ~75% of intact molecules (minus the N-terminus) even after incubation for 24 h. This result highlighted a minor

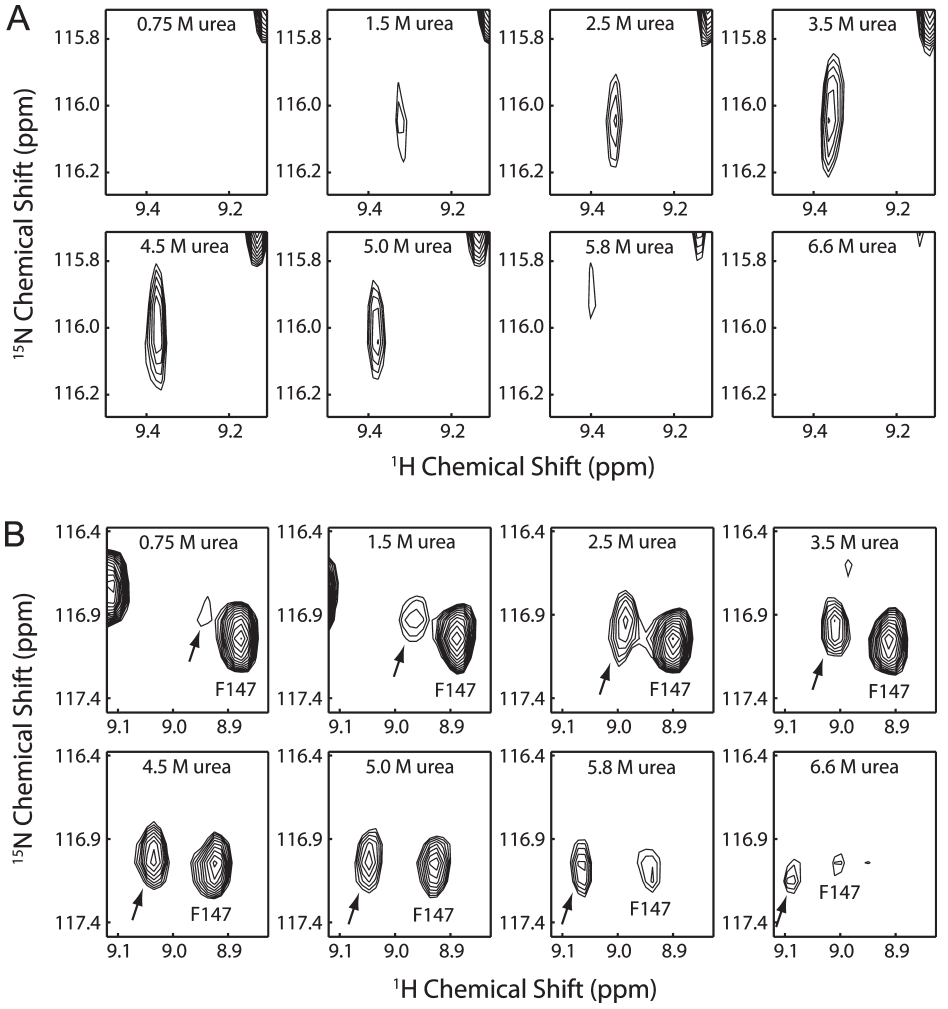


FIGURE 5: Expanded views of two $^{1}$H−$^{15}$N HSQC spectral regions of $^{13}$C- and $^{15}$N−labeled IL-1ra in the presence of different urea concentrations. In panel A, only the minor peak is shown. In panel B, the minor peak is indicated by an arrow. Residue assignments for the minor peaks are currently unavailable. Urea concentrations were 0.75, 1.5, 2.5, 3.5, 4.5, 5.0, 5.8, and 6.6 M (as indicated). Note that the intensities of the minor peaks are maximal in ~4 M urea.

role of the N-terminal segment in determining the structural stability of IL-1ra. In 3 M urea, the protein was only slightly less resistant and contained ~50% of intact molecules by the end of the study. In contrast, in 5 M urea, IL-1ra was ~90% digested already within the first 10 h due to unfolding. We analyzed the rate of protein fragmentation (represented by the percent loss of intact molecules) and compared it with the rate of unfolding in the absence of proteinase K. We found that IL-1ra unfolding did not accelerate in the digestion experiment (cf. $\sim 4 \times 10^{-5}$ s$^{-1}$ vs $\sim 6 \times 10^{-5}$ s$^{-1}$ in the absence of the protease), indicating little interference from the protease.

Despite the multiplicity of cleavage sites characteristic of proteinase K, the identification of peptides was near 100% because of highly resolving mass spectrometry (see Materials and Methods). Although in some cases peak coelution was observed, the peptides were identified with a high degree of confidence on the basis of their molecular mass and MS/MS fragmentation (see Table S1 of the Supporting Information). Thirty-five different cleavage sites were detected and mapped onto the crystal structure of IL-1ra (see Figure 7C). A large number of sites corresponded to partly exposed or buried peptide bonds, which likely gained accessibility upon digestion-induced disruption of the tertiary structure. The remaining solvent-exposed sites correlated well with the peptides, which showed higher abundance in 3 M urea compared to native conditions (see Figure S4 of the Supporting Information). They are illustrated in red in Figure 7C and listed in Table 3 along with the corresponding chromatographic peaks. Many of them resided within trefoils 1 and 2, primarily in the loop regions near the $3_{10}$ helices (see Discussion). These results were consistent with locally destabilized folded conformations of IL-1ra in 3 M urea.

*Optical Spectroscopy Analysis of W17A IL-1ra.* Additional evidence of noncooperative changes in IL-1ra was obtained using its previously constructed W17A mutant (*10*). Wild-type IL-1ra contains two tryptophan residues, Trp17 and Trp120, that are distant from each other within the protein structure. Among them, Trp17 is a dominant chromophore determining the fluorescence and CD properties of the protein (*10*). Trp17 exhibits no sensitivity toward the noncooperative changes, and its replacement with alanine is tolerated well by the protein structure (*10*). Therefore, the W17A mutant was found to be useful for investigating structural changes masked by the presence of Trp17.

Between 0 and 2 M urea, the tryptophan emission of W17A was fully quenched and the fluorescence spectra were dominated by the tyrosine band at 302 nm (Figure 6A). The addition of 3−4 M urea led to a partial recovery of the Trp120 emission, which exhibited several bands spanning the range of 335−350 nm.

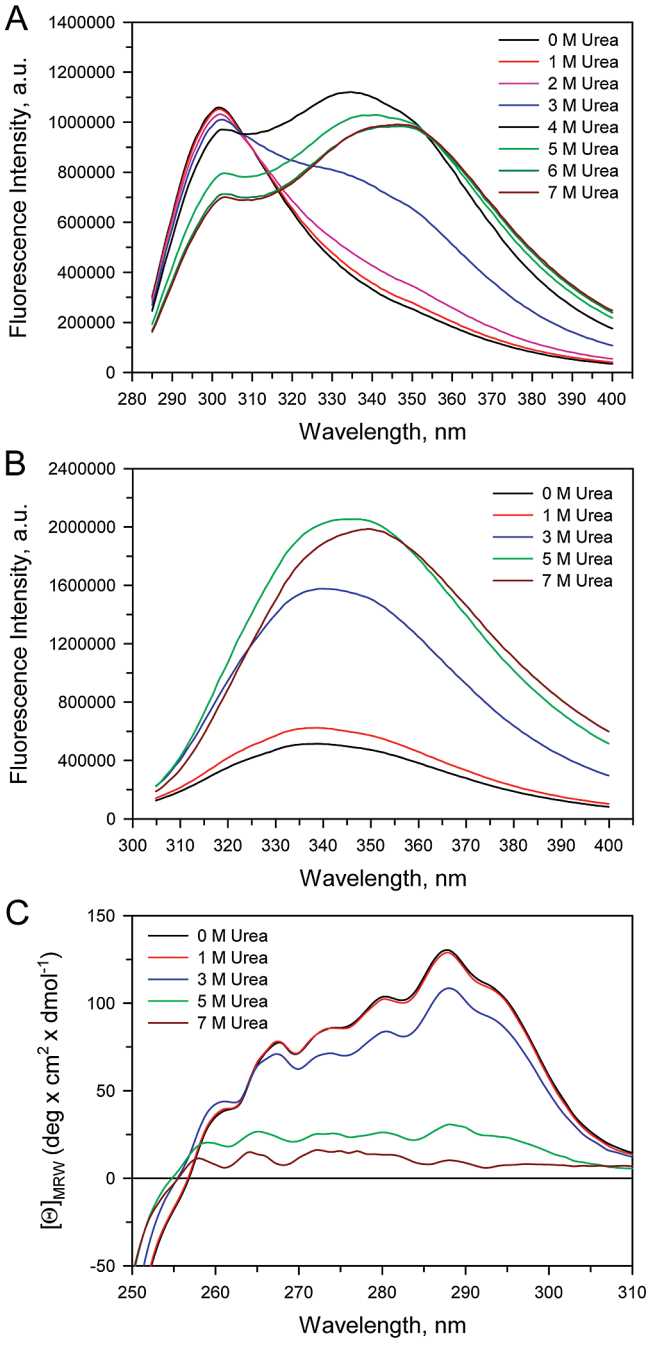


FIGURE 6: Optical spectroscopy measurements of W17A IL-1ra. (A) Fluorescence spectra as a function of urea concentration (excitation at 275 nm). (B) Fluorescence spectra as a function of urea concentration (excitation at 295 nm). (C) Near-UV CD spectra as a function of urea concentration.

The increase in tryptophan fluorescence was independent of the tyrosine excitation, as evidenced by the spectra collected with excitation wavelengths set to 275 and 295 nm (cf. Figure 6A,B). Since W17A is natively folded (*10*) and Trp17 and Trp120 are well separated within the $\beta$-trefoil structure, the data revealed denaturant-dependent loss of local quenching interactions rather than long-range mutational effects. To rule out the possibility that specific binding of urea to the native protein is responsible for this phenomenon, we conducted a series of experiments using GuHCl as a denaturant and obtained similar results (data not shown). To independently assess the extent of structural perturbation, we recorded near-UV CD spectra under identical conditions (Figure 6C). In agreement with the fluorescence data, no spectral changes were seen between 0 and 1 M urea and the addition of 3 M urea induced only minor changes consistent with a small-scale structural perturbation. To verify that these results were not influenced by protein aggregation, we performed analytical ultracentrifugation experiments under similar conditions (unpublished results by R. F. Latypov and V. I. Razinkov). No evidence of protein−protein association was found, and the frictional ratios remained essentially constant (1.3−1.4) up to 3 M urea. In contrast, fluorescence anisotropy measurements revealed increased Trp120 dynamics prior to global unfolding induced by both urea and GuHCl (data not shown). This decrease in tryptophan anisotropy was distinct from the anisotropy of the tyrosines, which showed virtually no changes. Therefore, the results for W17A confirmed accumulation of locally perturbed nativelike states prior to global unfolding.

Table 3: Limited Proteolysis of IL-1ra by Proteinase K and Structural Location of the Digestion "Hot Spots" That Differentiate Protein Samples Containing 0 and 3 M Urea

| cleavage site | peak[a] | secondary structure[b] | $\beta$-trefoil[b] |
|---|---|---|---|
| Asn20−Gln21 | 10[c] | loop region | 1 |
| Lys22−Thr23 | 8 | loop region/$\beta$2 strand | 1 |
| Asn42−Leu43 | 14 | H1 $3_{10}$ helix | 1 |
| His62−Gly63 | 13[c] | loop region | 2 |
| Val84−Asn85 | 10[c] | loop region | 2 |
| Thr87−Asp88 | 5[c] | H2a $3_{10}$ helix | 2 |
| Arg103−Ser104 | 5,[c] 6, 12 | $\beta$8 strand | 2 |
| Ala115−Ala116 | 15, 21 | loop region | 3 |

[a]Chromatographic peaks are numbered according to Figure S4 of the Supporting Information (several peaks containing one common cleavage site are listed together). More information about the peaks and peptides can be found in Table S1 of the Supporting Information. [b]Based on the crystal structure of IL-1ra (*9*). [c]This peak contained coeluting peptides (see Table S1 of the Supporting Information).

The fluorescence spectra of W17A exhibited two well-defined isosbestic points at 307 and 353.5 nm (Figure 6A), which provided further evidence of a non-two-state denaturation process. The first transition was associated with only limited structural changes. Our preliminary assessment showed that these changes were consistent with the appearance of the minor NMR peaks in a slow conformational exchange (see above). The second transition coincided with the global unfolding of the protein and thus corresponded to a transition between the overall folded and fully unfolded states. A more detailed analysis of W17A folding and unfolding will be presented elsewhere.

*NMR-Detected Structural Perturbations between 5 and 45 °C.* A brief overview of the temperature ramping data on $^{2}$H-, $^{13}$C-, and $^{15}$N-labeled IL-1ra was presented previously (*7*). The protein sample was heated from 5 to 45 °C, and a series of $^{1}$H−$^{15}$N HSQC spectra was recorded with 5 °C increments. Since this temperature range corresponded to conditions dominated by the folded state (*3*, *10*), this study helped to reveal residues accessing alternative conformations within a distance of 2−3 kcal/mol from the native state (*37*). Only ~80 native resonances were analyzed in this experiment because some of the cross-peaks appeared or disappeared as a function of temperature (other reasons for limited data included partial peak overlaps and missing assignments). The following peaks were identified on the basis of their pronounced nonlinear $^{1}$H chemical shift variations with temperature (with linear fit residuals exceeding or equal to ±0.01 ppm): Phe14, Arg15, Phe24, Gly34, Lys46, Lys65, Gln80, Ser90, and Glu91 (data not shown). This provided evidence of temperature-induced perturbations associated with

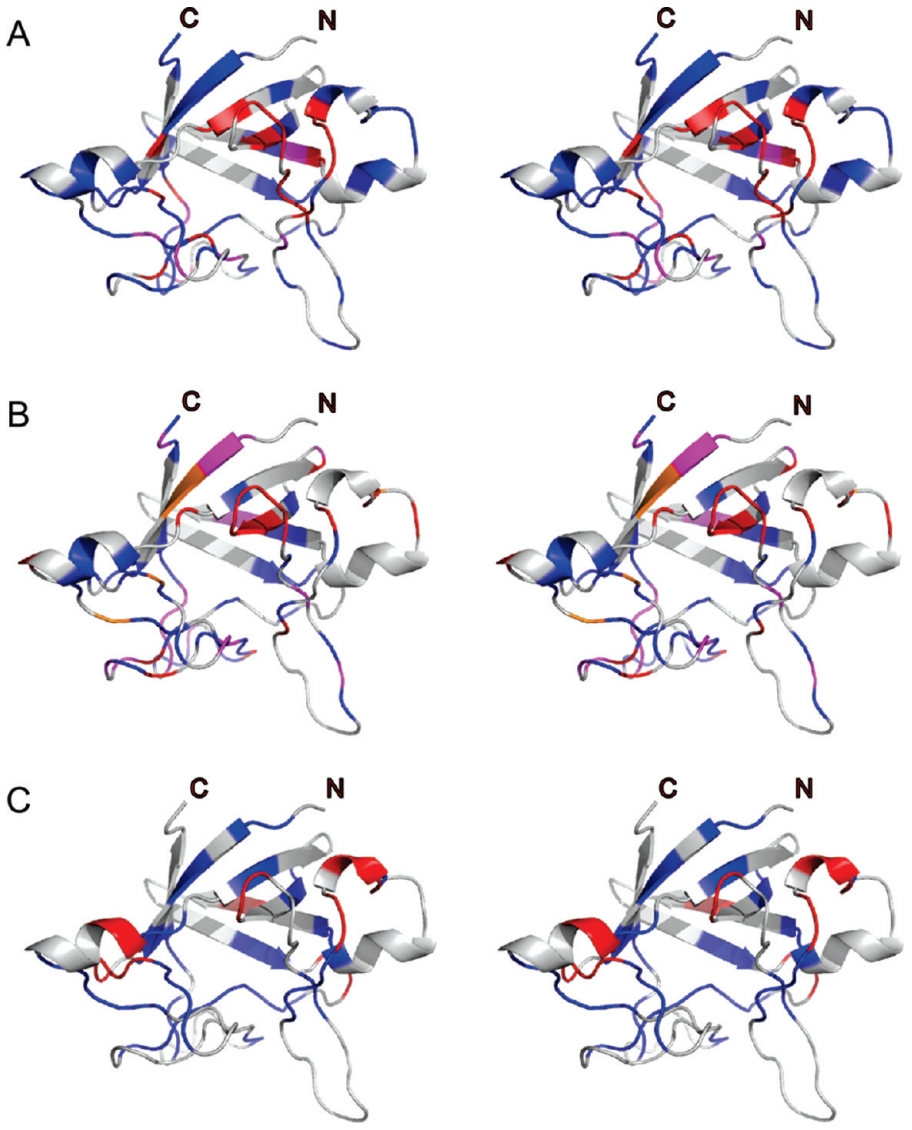


FIGURE 7: Stereo images of IL-1ra [PDB entry 1ILR (*9*)] illustrating urea- and temperature-induced perturbations in the protein. The molecule is oriented to show the interface between $\beta$-trefoils 1 and 2. The $\beta$-barrel is on the top, and the hairpin cap is at the bottom; the H1 helix is on the left, and the H2a−H2 helices are on the right. (A) Effect of 3.5 M urea on the protein structure based on $^{1}H-^{15}N$ HSQC NMR. Unperturbed residue positions for which resonance data are available are colored blue. Residues colored pink undergo $^{1}HN$ or $^{15}N$ chemical shift changes exceeding 0.1 or 0.5 ppm, respectively (Figure 3A,B). Residues colored red exhibit noncooperative (nonsigmoidal) peak intensity changes with urea (Figure 4A and Table 2). (B) Effect of temperature on the protein structure based on $^{1}H-^{15}N$ HSQC NMR. Unperturbed residue positions for which resonance data are available are colored blue. Residues colored pink undergo $^{1}HN$ or $^{15}N$ chemical shift changes exceeding 0.1 or 0.5 ppm, respectively, between 25 and 45 °C (Figure 3E,F). Residues colored red exhibit significant peak intensity changes between 5 and 45 °C. Residues colored orange undergo nonlinear $^{1}H$ chemical shift variations with temperature. (C) Effect of 3 M urea on limited proteolysis by proteinase K from real-time reversed-phase HPLC−MS analysis. The cleavage sites for which peptide data are available are colored blue. Residues colored red identify cleavage sites more accessible in 3 M urea than under native conditions (Table 3). The N- and C-termini are indicated. The figures were generated using PyMOL (DeLano Scientific LLC, South San Francisco, CA).

residue positions within the $\beta$1 and $\beta$4 strands, the $\beta$2−$\beta$3 and $\beta$6−$\beta$7 hairpins, and the H2a−H2 helices (see Figure 7B and Discussion).

Panels C−F of Figure 3 illustrate the effect of temperature on the $^{1}H$ and $^{15}N$ chemical shifts from the same experiment. Nondenaturing temperatures, such as 40−42 °C, were previously shown to induce irreversible aggregation of highly concentrated IL-1ra (*3*). These observations led to a hypothesis that elevated temperatures increased the population of partially unfolded molecules (*4*). To assess differences between the effects of cold and warm temperatures, data were purposely split into two temperature ranges, 5−25 (cold) and 25−45 °C (warm). Whereas both temperature variations induced comparable structural perturbations, the following residue positions deviated significantly between these two regimes in terms of either $^{1}H$ or $^{15}N$ chemical shifts: Phe14, Phe24, Lys46, Leu59, Lys65, Val71, Lys72, Ser90, Glu91, and Glu151. In addition, we observed substantial $^{15}N$ chemical shift changes at residues Ile61 and His62, for which no cross-peaks were present at temperatures below 20 °C (cf. Figure 3D,F). Overall, the data showed that higher temperatures induced perturbations primarily in the $\beta$1, $\beta$4, and $\beta$5 strands, the $\beta$2−$\beta$3 and $\beta$6−$\beta$7 hairpins, and the H2a−H2 helices (Figure 7B and Discussion).

In addition, peaks for the following positions exhibited large intensity variations between 5 and 45 °C: Gly38, Lys46, Ile52, Leu59, Gly60, Ile61, His62, Gly63, Gly64, Lys65, Gln80, Asn85, Leu89, Ser90, Arg93, Ala125, Gln130, and Asn136. Some of them appeared only upon heating, suggesting that they were in

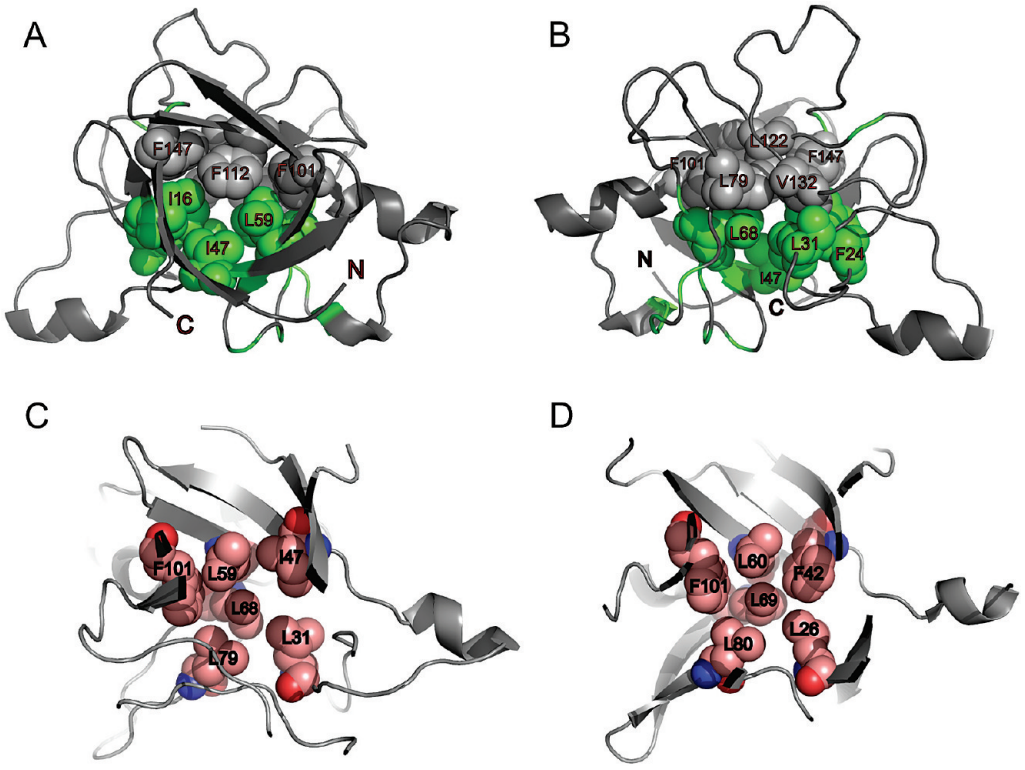


FIGURE 8: (A and B) Ribbon diagrams of IL-1ra [PDB entry 1ILR (*9*)] illustrating the location of noncooperative perturbations in the protein (green). Views from (A) the $\beta$-barrel and (B) the hairpin cap (the molecule is oriented with the $\beta$-barrel perpendicular to the plane of the page). Residues shown as spheres indicate core residues forming the interface between the cap and the $\beta$-barrel (see Table 4) (*11*). The majority of noncooperatively unfolding positions are located within trefoils 1 and 2 (see the text and Table 2). The N- and C-termini are indicated. (C and D) Differences in the core packing interactions between (C) IL-1ra and (D) IL-1$\beta$ [PDB entry 1I1B (*12*)]. Protein structures were similarly oriented and clipped to allow focusing on the interior residues. As a result of the aliphatic−aromatic switch (see the text and Table 4), the distance between the side chains of Ile47 and Leu31/Leu68 in IL-1ra has increased. In contrast, IL-1$\beta$ exhibits well-formed interlocking interactions between Leu26, Phe42, and Leu69. The figures were generated using PyMOL.

intermediate exchange at cold temperatures. Warming caused them to sharpen and become visible, indicating temperature-dependent changes in the protein structure and/or dynamics. Most of them resided within the same structural regions, which exhibited noncooperative perturbations with urea (Tables 2 and 3 and Figure 7A−C).

## DISCUSSION

Previous reports provided little information for understanding the role of protein structural changes in IL-1ra aggregation. One scenario suggested that IL-1ra aggregated via partially unfolded conformations populating in response to various stress factors, such as elevated temperature or destabilizing additives (benzyl alcohol, ANS, etc.) (*2*, *4*). However, detection and characterization of such partially denatured conformations proved to be difficult. The commonly used approaches based on intrinsic fluorescence and CD did not reveal any equilibrium intermediates populated to a measurable degree (*10*). The use of ANS provided no evidence of any significant changes in the exposure of hydrophobic surfaces (*7*, *10*), which is known to be a common signature of the molten globule states, yet H−D exchange experiments were consistent with a relatively dynamic protein conformation that was sensitive to the presence of different excipients (*2*). Results from this study helped to identify the location and magnitude of structural perturbations in IL-1ra under moderately destabilizing conditions. These previously unknown aspects are important for understanding the conformational flexibility of IL-1ra as a function of solution composition and temperature.

*Equilibrium Unfolding of IL-1ra*. IL-1ra was seen as a compact globular protein with an $R_g$ of ~17 Å in the presence of either 0−1 M GuHCl or 0−4 M urea (Figures 1 and 2). In agreement with this, the $^1H-^{15}N$ HSQC spectra exhibited similar chemical shift dispersion and line widths within the entire pretransition region indicative of a tightly folded protein structure (Figure S1 of the Supporting Information). The results of the real-time proteinase K digestion experiments were consistent with an ensemble of protease-resistant protein conformations up to 3−5 M urea (see Results and Figure S4 of the Supporting Information). These findings provided compelling evidence of a largely intact protein conformation within its native baseline region. However, high-resolution NMR and limited proteolysis did provide evidence of some localized changes in the folded protein. We have found that the hairpin cap of IL-1ra is particularly susceptible to structural and dynamic changes at moderate denaturant concentrations. Also, we have identified a large cluster of noncooperatively unfolding positions primarily from trefoils 1 and 2 (see the detailed discussion below). This cluster is located slightly outside of the potential disulfide bridge between Cys70 and Cys117 (*9*), which was kept reduced at all times throughout the experiments. The specific location of the cluster made it silent to optical spectroscopy, explaining the lack of evidence from previous fluorescence and CD measurements (*2*, *4*, *10*). In particular, the dominant Trp17 is insensitive to such structural perturbations since it is located outside of the perturbed region. On the other hand, Trp120 fluorescence cannot serve as a useful probe as it is quenched in the folded state. Tryptophan contributions to IL-1ra CD, including the far-UV

region, are also known to be dominated by Trp17 (*10*). Therefore, detection of such structural changes by optical techniques was not possible without the use of the W17A mutant.

Noncooperative structural changes under mildly denaturing conditions were described for a number of small globular proteins and leucine zipper peptides. Hilser et al. provided computational evidence of the non-two-state nature of small single-domain proteins at equilibrium (*38*). In particular, the native state was seen as a statistical subensemble of conformations that exhibit local transitions. These conformations are predominantly folded globally but may be unfolded locally at certain residues (*19*). In the case of $\beta$-trefoil proteins, an increase in the conformational dynamics was generally observed, while populating equilibrium intermediates were reported only for hFGF-1 (*13*, *14*). Our new results for IL-1ra contribute to this observation by revealing another highly nativelike intermediate, which is distinct from the native state in the absence of denaturant.

Among $\beta$-trefoil proteins, the most detailed equilibrium unfolding characterization is available for IL-1$\beta$ and hFGF-1 (*13*, *14*, *19*). Equilibrium unfolding of IL-1$\beta$ proceeds through an ensemble of hyperfluorescent nativelike states, which are populated within its native baseline region. Although these states were found to be conformationally flexible, their backbone dynamics were nativelike, and it was concluded that their hyperfluorescence stemmed from relatively subtle structural changes. Both IL-1$\beta$ and W17A IL-1ra contain structurally equivalent Trp120, which becomes highly fluorescent prior to unfolding. Therefore, our results for IL-1ra help us to understand protein-specific deviations from a cooperative unfolding mechanism, as well as the nature of protein hyperfluorescence.

We previously concluded that quenching of Trp120 in IL-1ra results from its proximity to Cys70 and Cys117 (*10*). Unfolding of the protein is concomitant with the growth of Trp120 fluorescence presumably due to an increased time-averaged distance of the tryptophan from Cys70 (*10*). Because of local structural rearrangements (or side chain reorientations), the efficiency of quenching may decrease upon the formation of the nativelike intermediate observed in this study. This is possible because Trp120 is packed against the $\beta6-\beta7$ hairpin, which exhibits structural and dynamic changes prior to unfolding (see Results and Table 2). Among the two cysteine residues present in IL-1$\beta$, Cys8 and Cys71, the latter is structurally equivalent to Cys70 in IL-1ra. On the basis of its similar orientation and proximity to the sole Trp120, Cys71 of IL-1$\beta$ may act as a quencher of protein fluorescence. Structural perturbations in IL-1$\beta$ modulated by low denaturant concentrations may affect native quenching interactions leading to formation of the hyperfluorescent states. The commonality of structural features of the hyperfluorescent states of IL-1ra and IL-1$\beta$ further supports this scenario. Such interpretation also helps to address an apparent distinction in the equilibrium unfolding mechanisms of IL-1$\beta$ and hFGF-1. Although the latter is not hyperfluorescent, judging from the NMR and limited proteolysis data, it possesses a highly nativelike intermediate resembling the nativelike state of IL-1ra (*14*). Analysis of the hFGF-1 crystal structure [PDB entry 2AXM (*39*)] reveals that this protein does not contain cysteines equivalent to Cys70 in IL-1ra or Cys71 in IL-1$\beta$, although its sole Trp107 is equivalent to Trp120 in these two proteins. The tryptophan quenching effect in hFGF-1 is attributed to the presence of proximal His102 and Pro121, which may respond differently to small-scale structural perturbations. Moreover, structural perturbations in hFGF-1 are predominantly located within trefoil 3, rather than trefoil 1 or 2 (*14*). Therefore, it is not surprising that the unfolding equilibrium of hFGF-1 possesses nativelike states manifested differently from those of IL-1ra or IL-1$\beta$. On the basis of such comparative analysis, accumulation of highly nativelike intermediates (or native subconformations) in the case of $\beta$-trefoil proteins may be a general phenomenon.

Localized structural perturbations in the folded ensemble also have implications for IL-1ra kinetic unfolding measurements and data interpretation. Previous real-time NMR experiments on IL-1$\beta$ revealed heterogeneity in its individual amino acid residue kinetics, which suggested a rugged energy landscape for unfolding (*40*). The urea-induced unfolding of the protein was seen as a slow noncooperative process controlled by short-range interactions. Because of the high degree of structural similarity, IL-1ra also unfolds slowly (*10*) and can be studied by real-time 2D NMR. Our preliminary $^{1}H-^{15}N$ HSQC assessment of its unfolding kinetics (NMR experiments by R. F. Latypov, T. S. Harvey, and D. Liu, unpublished results) showed that by the time of the first spectral acquisition (within ~10 min of mixing the protein with urea) a number of native resonances disappeared while protein remained as compact and globular as in the absence of urea (time-resolved SAXS measurements by R. F. Latypov and D. Liu, unpublished results). In agreement with the equilibrium data, many of these early disappearing peaks were associated with the same structurally flexible regions (a more detailed analysis of the kinetic data will be presented elsewhere). Following this initial change, the unfolding process was seen as a very slow but cooperative transition on both global and residue-specific levels. Such NMR results suggested the presence of the same nativelike intermediate in the kinetic unfolding pathway of IL-1ra.

*Structural Perturbations and Protein Aggregation*. Comparison of the chemical shift data generated in the presence of various concentrations of urea or at different temperatures shows that these two factors may have different effects on the protein structure. The effect of urea appears to be largely mediated through its binding to the protein, particularly to the hairpin cap and surrounding regions. This is evidenced by the overall distribution of $^{15}N$ chemical shifts (Figure 3B), as well as many residues exhibiting urea binding type of $^{1}H$ chemical shift dependencies (Figure S2 of the Supporting Information). Changes in chemical shifts may reflect changes in hydrogen bonding, and there is a strong correlation between hydrogen bond energies and amide proton or amide nitrogen chemical shifts (*41*). The particularly large change in the $^{15}N$ chemical shift of His62 with temperature (Figure 3F) likely reflects changes in the interactions of this residue with solvent molecules. This is supported by the analysis of two crystal structures of IL-1ra [PDB entries 1ILR (*9*) and 1IRA (*42*)], which display water molecules hydrogen bonded to the amide nitrogen of His62.

Despite some disparity between the urea and temperature data, our results are suggestive of similar structural transitions in both cases. For example, the noncooperative perturbations induced by urea involved residues accessing alternative conformations via temperature (cf. red in Figure 7A and orange in Figure 7B). The same regions gained accessibility for the protease cleavage in 3 M urea (Table 3) or contained residues exhibiting large peak intensity variations between cold and warm temperatures (cf. red in Figure 7B and red in Figure 7C). Notably, they also harbored two solvent inaccessible cysteines, Cys67 and Cys70, which gained reactivity only at elevated temperatures or

Table 4: Structurally Equivalent Core Residues of IL-1ra and IL-1$\beta$ That Form Interlocking Interactions between the $\beta$-Barrel and the Hairpin Cap[a]

| protein | bottom layer of the $\beta$-barrel[b,c] | upper layer of the hairpin cap[c] | lower layer of the hairpin cap |
|---|---|---|---|
| IL-1ra | $^{16}$I--$^{47}$*I*--$^{59}$L--$^{101}$**F**--$^{112}$F--$^{147}$**F** | $^{24}$*F*--$^{68}$L--$^{122}$L | $^{31}$L--$^{79}$L--$^{132}$V |
| IL-1$\beta$ | $^{10}$L--$^{42}$**F**--$^{60}$L--$^{101}$**F**--$^{112}$F--$^{146}$**F** | $^{18}$L--$^{69}$L--$^{122}$I | $^{26}$L--$^{80}$L--$^{132}$V |

[a]Based on ref *11* and crystal structures from refs *9* and *12*. [b]The side chains from the $\beta$-barrel pointing toward the hairpin cap (i.e., the anchoring residues) are shown in bold (see the text). [c]IL-1ra residues that undergo the aliphatic−aromatic switch between the $\beta$-barrel and the hairpin cap are shown in italic (see the text).

in the presence of benzyl alcohol (*4*). These findings showed that noncooperative perturbations occurred within regions of localized conformational flexibility and could potentially play a role in protein aggregation. For example, Lys94 was previously identified as a key residue involved in IL-1ra aggregation induced by elevated temperatures (*3*). It is a solvent-exposed residue located at the N-terminus of the H2 helix, in a chain segment adjacent to the $\beta$6−$\beta$7 hairpin. Also, aggregation of IL-1ra was accelerated in the presence of ANS (*4*), which targeted the H2a−H2 helical region including residues 90−97 (*7*). Thus, there is substantial experimental evidence linking less stable structural regions to the regions that control protein aggregation.

One of them is the H2a−H2 helical region, which does not belong to the symmetric $\beta$-trefoil framework and is packed against it. Residues that are directly or indirectly involved in its packing are: Met11, **Asp48**, Val50, Phe58, **Leu59**, **Gly63**, **Gly64**, **Cys67**, **Leu68**, **Ser69**, Cys70, **Glu82**, **Val84**, **Asn85**, **Ile86**, Leu89, Ser90, Arg93, Asp96, Lys97, Arg98, Phe99, **Ala100**, Phe101, Ala115, and Ala116. This list contains 12 of 20 residues listed in Table 2 (indicated here in bold), with three more residues for which no NMR data are available (Arg98, Phe99, and Ala116). Combined with the limited proteolysis data, which showed loss of protection at His62-Gly63, Val84-Asn85, Thr87-Asp88, Arg103-Ser104, and Ala115-Ala116 segments (Table 3), and colocalization of the temperature-induced changes, there is little doubt that most of the structural perturbations were associated with the packing of the H2a and H2 helices. In addition, data suggested propagation of structural changes into the core of the protein, particularly with respect to the $\beta$2−$\beta$3 hairpin and the $\beta$1 and $\beta$4 strands. To address this phenomenon, we compared details of packing interactions in IL-1ra and IL-1$\beta$.

IL-1ra and IL-1$\beta$ are structurally similar (*8*, *9*); however, IL-1$\beta$ does not exhibit well-defined localized perturbations (*19*). One key aspect that appears to be responsible for this difference is the absence of the H2a−H2 helices in IL-1$\beta$ [PDB entry 1I1B (*12*)]. Another important difference lies in their core regions and involves hydrophobic packing interactions between the $\beta$-barrel and the cap. The role of these interactions in determining the cooperativity of the $\beta$-trefoil structure was previously evaluated in the case of IL-1$\beta$ (*43*).

Within the $\beta$-trefoil structure, the interior side chains of the barrel are packed in regular arrays forming three layers: top, middle, and bottom (each containing six residues) (*11*). Three side chains from the bottom layer point toward the hairpin cap with which they make contact. The packing of side chains in the cap was also described in terms of layers: upper and lower (each containing three residues) (*11*). The upper layer side chains of the cap pack against the three bottom layer side chains from the barrel. In IL-1$\beta$, the side chains of Phe42, Phe101, and Phe146 point toward the cap and interlock with its aliphatic residues Leu18, Leu69, and Ile122 (see Table 4). In IL-1ra, structurally equivalent residues Ile47, Phe101, and Phe147 pack against Phe24, Leu68, and Leu122 from the cap (Table 4). Although generally similar, these packing interactions differ between IL-1ra and IL-1$\beta$ in the vicinity of Ile47 and Phe42, respectively (cf. Figure 8C,D). The hydrophobic core of IL-1$\beta$ is stabilized by a symmetric array of large and bulky phenylalanine side chains from the barrel packing against the aliphatic side chains of the cap. The same is true for IL-1ra except for the replacement of one of its anchoring phenylalanines with an isoleucine at position 47 (Table 4). As shown in Figure 8C, the consequence of this replacement is the lack of packing interactions between Ile47 and the cap (Leu31 and Leu68). We note another symmetry break within the upper layer of the cap: in contrast to IL-1$\beta$, with its fully aliphatic cap layers, IL-1ra contains Phe24 in place of a leucine. Although large and bulky, its side chain packs only against Leu31 and Ile47 while leaving a cavity between Ile47 and Leu68. The existence of this cavity may translate into a decrease in the level of mutual stabilization of trefoils 1 and 2 in IL-1ra. This aliphatic−aromatic switch between the bottom layer of the barrel and the upper layer of the cap (see Table 4) may be responsible for propagation of structural perturbations from the H2a−H2 helical region toward trefoil 1.

The existence of core packing defects in $\beta$-trefoil proteins is not uncommon (*44*), and some information about their role in protein stability and folding is available (*45*, *46*). Trefoils in $\beta$-trefoil proteins may exhibit domain motions even though they are symmetrically related regions that cannot be readily identified as separate domains. As a result, some regions of the $\beta$-trefoil structure may appear as relatively flexible separate subdomains (*44*). As follows from panels A and B of Figure 8, the cavity that is formed by Leu31, Ile47, and Leu68 is located at the center of the noncooperative cluster formed by the residues from Table 2. Although no direct evidence is currently available, we hypothesize that cooperativity of the IL-1ra structure depends on the quality of side chain packing interactions (*47*) and could be lost via a combination of factors. One is the intrinsic instability around the H2a and H2 helices, which makes this region structurally flexible; another is the presence of the aforementioned cavity in relative proximity to the helical region. Elevated temperatures that destabilize the H2a−H2 segment may weaken coupling between trefoils 1 and 2 and exacerbate the effect of the cavity. This may increase intertrefoil motions and lead to partial denaturation (presumably via unzipping of the $\beta$4 and $\beta$5 strands, and separation of the $\beta$2−$\beta$3 and $\beta$6−$\beta$7 hairpins), which would expose core regions of IL-1ra driving its aggregation process.

In contrast to FGF-1 (*44*), the biological relevance of noncooperative changes in IL-1ra is currently unknown as they do not reflect the receptor binding functionality of the protein (*42*). Nevertheless, there is good agreement between the urea-dependent and temperature-induced changes associated with the H2a−H2 helical region and surrounding areas. We also note that the H2a−H2 helical region contains the loop of residues 85−99 previously implicated in the asymmetric association of IL-1ra in solution (*3*) and crystal dimer formation (*9*). Thus, there is sufficient evidence to date of the involvement of specific parts of

the protein in modulating its solution behavior and aggregation. The effect of anions in weakening IL-1ra aggregation was mediated through their binding to the H2 helical region (*3*). It is possible that self-association of IL-1ra represents a way of protein stabilization driven by interactions involving the same helical regions. Indeed, highly concentrated IL-1ra was shown to exist in a monomer−dimer equilibrium controlled by interactions consistent with those found in the crystal dimer (*5*, *6*).

*Denaturant Dependence of Unfolded Conformations*. It has been suggested that milder conditions favor more compact protein-denatured states (*48*), and the unfolded ensemble was recognized as being critical in defining protein folding kinetics and thermodynamics (*29*). Experimental data suggested that unfolded proteins may contain residual structures stabilized by either hydrophobic (*49*−*52*) or electrostatic interactions (*53*, *54*). However, experimental confirmation of this behavior has often come from FRET-based studies (*55*, *56*) and not from SAXS (*30*, *57*). Therefore, our comparative analysis of the SAXS data for the urea- and GuHCl-denatured IL-1ra provides valuable information. The $R_g$ of the unfolded protein increases gradually over a wide range of GuHCl concentrations (Figures 1C and 2A). The post-transition region linearly extrapolates to zero denaturant and gives an $R_g$ value ~15% smaller (35.4 ± 0.6 Å) than that measured under strongly denaturing conditions (~41 Å). Also, the $R_g$ values of the urea- and GuHCl-denatured molecules differ at lower denaturant concentrations (Figure 2A), suggesting the possibility of an incomplete destabilization of intramolecular interactions within the unfolded state ensemble. Although it is generally accepted that SAXS measurements do not provide evidence of any appreciable chain expansion beyond the unfolding transition region (*30*, *57*), our data and results from a recent study on the urea-denatured dihydrofolate reductase (*33*) clearly deviate from this rule.

## ACKNOWLEDGMENT

We thank Jeffrey Lewis, Tadahiko Kohno, James Zondlo, Jane Talvenheimo, and Thomas C. Boone at Amgen Inc. for their help with the expression and purification of the isotopically enriched human recombinant IL-1ra and Prof. Melanie Cocco (University of California, Irvine, CA) for her assistance in acquiring the NMR data. We are grateful to Heinrich Roder, Kannan Gunasekaran, Vladimir I. Razinkov, Songpon Deechongkit, Yatin R. Gokarn, Scott Silbiger, Bruce A. Kerwin, and Michael J. Treuheit for their help with the manuscript, expert advice, and fruitful discussions. We also thank Liang Guo (BioCAT, Advanced Photon Source) for valuable technical assistance with the SAXS measurements and Jared M. Trefethen (Texas A&M University, College Station, TX) and Nick Van Buren (Amgen Inc.) for their help with the equilibrium titration experiments. Use of the Advanced Photon Source was supported by the U.S. Department of Energy, Basic Energy Sciences, Office of Science, under Contract 2006-03216. BioCAT is a research center supported by the National Institutes of Health.

## SUPPORTING INFORMATION AVAILABLE

$^1H-^{15}N$ HSQC spectra of IL-1ra in the absence and presence of urea (Figure S1), representative $^1H$ chemical shift variations of the native amide resonances as a function of urea concentration (Figure S2), $^1H-^{15}N$ HSQC spectral regions demonstrating the disappearance of the native amide peaks of Cys67 and Glu82 with an increase in urea concentration (Figure S3), reversed-phase HPLC separation of IL-1ra peptides generated by proteinase K (Figure S4), and a summary of peptide identification based on molecular mass and MS/MS fragmentation data (Table S1). This material is available free of charge via the Internet at http://pubs.acs.org.

## REFERENCES

1. Dinarello, C. A. (1996) Biologic basis for interleukin-1 in disease. *Blood 87*, 2095–2147.
2. Zhang, Y., Roy, S., Jones, L. S., Krishnan, S., Kerwin, B. A., Chang, B. S., Manning, M. C., Randolph, T. W., and Carpenter, J. F. (2004) Mechanism for benzyl alcohol-induced aggregation of recombinant human interleukin-1 receptor antagonist in aqueous solution. *J. Pharm. Sci. 93*, 3076–3089.
3. Raibekas, A. A., Bures, E. J., Siska, C. C., Kohno, T., Latypov, R. F., and Kerwin, B. A. (2005) Anion binding and controlled aggregation of human interleukin-1 receptor antagonist. *Biochemistry 44*, 9871–9879.
4. Roy, S., Katayama, D., Dong, A., Kerwin, B. A., Randolph, T. W., and Carpenter, J. F. (2006) Temperature dependence of benzyl alcohol- and 8-anilinonaphthalene-1-sulfonate-induced aggregation of recombinant human interleukin-1 receptor antagonist. *Biochemistry 45*, 3898–3911.
5. Alford, J. R., Kwok, S. C., Roberts, J. N., Wuttke, D. S., Kendrick, B. S., Carpenter, J. F., and Randolph, T. W. (2008) High concentration formulations of recombinant human interleukin-1 receptor antagonist: I. Physical characterization. *J. Pharm. Sci. 97*, 3035–3050.
6. Alford, J. R., Kendrick, B. S., Carpenter, J. F., and Randolph, T. W. (2008) High concentration formulations of recombinant human interleukin-1 receptor antagonist: II. Aggregation kinetics. *J. Pharm. Sci. 97*, 3005–3021.
7. Latypov, R. F., Liu, D., Gunasekaran, K., Harvey, T. S., Razinkov, V. I., and Raibekas, A. A. (2008) Structural and thermodynamic effects of ANS binding to human interleukin-1 receptor antagonist. *Protein Sci. 17*, 652–663.
8. Eisenberg, S. P., Evans, R. J., Arend, W. P., Verderber, E., Brewer, M. T., Hannum, C. H., and Thompson, R. C. (1990) Primary structure and functional expression from complementary DNA of a human interleukin-1 receptor antagonist. *Nature 343*, 341–346.
9. Schreuder, H. A., Rondeau, J. M., Tardif, C., Soffientini, A., Sarubbi, E., Akeson, A., Bowlin, T. L., Yanofsky, S., and Barrett, R. W. (1995) Refined crystal structure of the interleukin-1 receptor antagonist. Presence of a disulfide link and a *cis*-proline. *Eur. J. Biochem. 227*, 838–847.
10. Latypov, R. F., Harvey, T. S., Liu, D., Bondarenko, P. V., Kohno, T., Fachini, R. A.II, Rosenfeld, R. D., Ketchem, R. R., Brems, D. N., and Raibekas, A. A. (2007) Biophysical characterization of structural properties and folding of interleukin-1 receptor antagonist. *J. Mol. Biol. 368*, 1187–1201.
11. Murzin, A. G., Lesk, A. M., and Chothia, C. (1992) $\beta$-Trefoil fold. Patterns of structure and sequence in the Kunitz inhibitors interleukins-1$\beta$ and 1$\alpha$ and fibroblast growth factors. *J. Mol. Biol. 223*, 531–543.
12. Finzel, B. C., Clancy, L. L., Holland, D. R., Muchmore, S. W., Watenpaugh, K. D., and Einspahr, H. M. (1989) Crystal structure of recombinant human interleukin-1$\beta$ at 2.0 Å resolution. *J. Mol. Biol. 209*, 779–791.
13. Samuel, D., Kumar, T. K. S., Srimathi, T., Hsieh, H.-C., and Yu, C. (2000) Identification and characterization of an equilibrium intermediate in the unfolding pathway of an all $\beta$-barrel protein. *J. Biol. Chem. 275*, 34968–34975.
14. Srimathi, T., Kumar, T. K. S., Chi, Y.-H., Chiu, I.-M., and Yu, C. (2002) Characterization of the structure and dynamics of a near-native equilibrium intermediate in the unfolding pathway of an all $\beta$-barrel protein. *J. Biol. Chem. 277*, 47507–47516.
15. Estapé, D., and Rinas, U. (1999) Folding kinetics of the all-$\beta$-sheet protein human basic fibroblast growth factor, a structural homolog of interleukin-1$\beta$. *J. Biol. Chem. 274*, 34083–34088.
16. Liu, C., Gaspar, J. A., Wong, H. J., and Meiering, E. M. (2002) Conserved and nonconserved features of the folding pathway of hisactophilin, a $\beta$-trefoil protein. *Protein Sci. 11*, 669–679.
17. Chavez, L. L., Gosavi, S., Jennings, P. A., and Onuchic, J. N. (2006) Multiple routes lead to the native state in the energy landscape of the $\beta$-trefoil family. *Proc. Natl. Acad. Sci. U.S.A. 103*, 10254–10258.
18. Capraro, D. T., Roy, M., Onuchic, J. N., and Jennings, P. A. (2008) Backtracking on the folding landscape of the $\beta$-trefoil protein interleukin-1$\beta$? *Proc. Natl. Acad. Sci. U.S.A. 105*, 14844–14848.

19. Roy, M., Chavez, L. L., Finke, J. M., Heidary, D. K., Onuchic, J. N., and Jennings, P. A. (2005) The native energy landscape for interleukin-1$\beta$. Modulation of the population ensemble through native-state topology. *J. Mol. Biol. 348*, 335–347.
20. Glatter, O., and Kratky, O. (1982) Small Angle X-ray Scattering, Academic Press, London.
21. Kataoka, M., Nishii, I., Fujisawa, T., Ueki, T., Tokunaga, F., and Goto, Y. (1995) Structural characterization of the molten globule and native states of apomyoglobin by solution X-ray scattering. *J. Mol. Biol. 249*, 215–228.
22. Delaglio, F., Grzesiek, S., Vuister, G. W., Zhu, G., Pfeifer, J., and Bax, A. (1995) NMRPipe: A multidimensional spectral processing system based on UNIX pipes. *J. Biomol. NMR 6*, 277–293.
23. Johnson, B. A. (2004) Using NMRView to visualize and analyze the NMR spectra of macromolecules. *Methods Mol. Biol. 278*, 313–352.
24. Stockman, B. J., Scahill, T. A., Roy, M., Ulrich, E. L., Strakalaitis, N. A., Brunner, D. P., Yem, A. W., and Deibel, M. R. Jr. (1992) Secondary structure and topology of interleukin-1 receptor antagonist protein determined by heteronuclear three-dimensional NMR spectroscopy. *Biochemistry 31*, 5237–5245.
25. Dillon, T. M., Bondarenko, P. V., Rehder, D. S., Pipes, G. D., Kleemann, G. R., and Ricci, M. S. (2006) Optimization of a reversed-phase high-performance liquid chromatography/mass spectrometry method for characterizing recombinant antibody heterogeneity and stability. *J. Chromatogr., A 1120*, 112–120.
26. Ren, D., Pipes, G. D., Liu, D., Shih, L. Y., Nichols, A. C., Treuheit, M. J., Brems, D. N., and Bondarenko, P. V. (2009) An improved trypsin digestion method minimizes digestion-induced modifications on proteins. *Anal. Biochem. 392*, 12–21.
27. Guinier, A., and Fournet, G. (1955) Small Angle Scattering of X-rays, Wiley, New York.
28. Kataoka, M., Hagihara, Y., Mihara, K., and Goto, Y. (1993) Molten globule of cytochrome *c* studied by small angle X-ray scattering. *J. Mol. Biol. 229*, 591–596.
29. Millett, I. S., Doniach, S., and Plaxco, K. W. (2002) Toward a taxonomy of the denatured state: Small angle scattering studies of unfolded proteins. *Adv. Protein Chem. 62*, 241–262.
30. Kohn, J. E., Millett, I. S., Jacob, J., Zagrovic, B., Dillon, T. M., Cingel, N., Dothager, R. S., Seifert, S., Thiyagarajan, P., Sosnick, T. R., Hasan, M. Z., Pande, V. S., Ruczinski, I., Doniach, S., and Plaxco, K. W. (2004) Random-coil behavior and the dimensions of chemically unfolded proteins. *Proc. Natl. Acad. Sci. U.S.A. 101*, 12491–12496.
31. Semisotnov, G. V., Kihara, H., Kotova, N. V., Kimura, K., Amemiya, Y., Wakabayashi, K., Serdyuk, I. N., Timchenko, A. A., Chiba, K., Nikaido, K., Ikura, T., and Kuwajima, K. (1996) Protein globularization during folding. A study by synchrotron small-angle X-ray scattering. *J. Mol. Biol. 262*, 559–574.
32. Chen, L., Hodgson, K. O., and Doniach, S. (1996) A lysozyme folding intermediate revealed by solution X-ray scattering. *J. Mol. Biol. 261*, 658–671.
33. Arai, M., Kondrashkina, E., Kayatekin, C., Matthews, C. R., Iwakura, M., and Bilsel, O. (2007) Microsecond hydrophobic collapse in the folding of *Escherichia coli* dihydrofolate reductase, an $\alpha/\beta$-type protein. *J. Mol. Biol. 368*, 219–229.
34. Pace, C. N. (1986) Determination and analysis of urea and guanidine hydrochloride denaturation curves. *Methods Enzymol. 131*, 266–280.
35. Uzawa, T., Akiyama, S., Kimura, T., Takahashi, S., Ishimori, K., Morishima, I., and Fujisawa, T. (2004) Collapse and search dynamics of apomyoglobin folding revealed by submillisecond observations of $\alpha$-helical content and compactness. *Proc. Natl. Acad. Sci. U.S.A. 101*, 1171–1176.
36. Fontana, A., de Laureto, P. P., Spolaore, B., Frare, E., Picotti, P., and Zambonin, M. (2004) Probing protein structure by limited proteolysis. *Acta Biochim. Pol. 51*, 299–321.
37. Baxter, N. J., Hosszu, L. L., Waltho, J. P., and Williamson, M. P. (1998) Characterisation of low free-energy excited states of folded proteins. *J. Mol. Biol. 284*, 1625–1639.
38. Hilser, V. J., Dowdy, D., Oas, T. G., and Freire, E. (1998) The structural distribution of cooperative interactions in proteins: Analysis of the native state ensemble. *Proc. Natl. Acad. Sci. U.S.A. 95*, 9903–9908.
39. DiGabriele, A. D., Lax, I., Chen, D. I., Svahn, C. M., Jaye, M., Schlessinger, J., and Hendrickson, W. A. (1998) Structure of a heparin-linked biologically active dimer of fibroblast growth factor. *Nature 393*, 812–817.
40. Roy, M., and Jennings, P. A. (2003) Real-time NMR kinetic studies provide global and residue-specific information on the non-cooperative unfolding of the $\beta$-trefoil protein, interleukin-1$\beta$. *J. Mol. Biol. 328*, 693–703.
41. Wishart, D. S., Sykes, B. D., and Richards, F. M. (1991) Relationship between nuclear magnetic resonance chemical shift and protein secondary structure. *J. Mol. Biol. 222*, 311–333.
42. Schreuder, H., Tardif, C., Trump-Kallmeyer, S., Soffientini, A., Sarubbi, E., Akeson, A., Bowlin, T., Yanofsky, S., and Barrett, R. W. (1997) A new cytokine-receptor binding mode revealed by the crystal structure of the IL-1 receptor with an antagonist. *Nature 386*, 194–200.
43. Heidary, D. K., and Jennings, P. A. (2002) Three topologically equivalent core residues affect the transition state ensemble in a protein folding reaction. *J. Mol. Biol. 316*, 789–798.
44. Bernett, M. J., Somasundaram, T., and Blaber, M. (2004) An atomic resolution structure for human fibroblast growth factor 1. *Proteins 57*, 626–634.
45. Covalt, J. C. Jr., Roy, M., and Jennings, P. A. (2001) Core and surface mutations affect folding kinetics, stability and cooperativity in IL-1$\beta$: Does alteration in buried water play a role? *J. Mol. Biol. 307*, 657–669.
46. Brych, S. R., Kim, J., Logan, T. M., and Blaber, M. (2003) Accomodation of a highly symmetric core within a symmetric protein superfold. *Protein Sci. 12*, 2704–2718.
47. Shakhnovich, E. I., and Finkelstein, A. V. (1989) Theory of cooperative transitions in protein molecules. I. Why denaturation of globular protein is a first-order phase transition. *Biopolymers 28*, 1667–1680.
48. Dill, K. A., and Shortle, D. (1991) Denatured states of proteins. *Annu. Rev. Biochem. 60*, 795–825.
49. Evans, P. A., Topping, K. D., Woolfson, D. N., and Dobson, C. M. (1991) Hydrophobic clustering in nonnative states of a protein: interpretation of chemical shifts in NMR spectra of denatured states of lysozyme. *Proteins 9*, 248–266.
50. Neri, D., Billeter, M., Wider, G., and Wüthrich, K. (1992) NMR determination of residual structure in a urea-denatured protein, the 434-repressor. *Science 257*, 1559–1563.
51. Lietzow, M. A., Jamin, M., Dyson, H. J., and Wright, P. E. (2002) Mapping long-range contacts in a highly unfolded protein. *J. Mol. Biol. 322*, 655–662.
52. Schwarzinger, S., Wright, P. E., and Dyson, H. J. (2002) Molecular hinges in protein folding: The urea-denatured state of apomyoglobin. *Biochemistry 41*, 12681–12686.
53. Oliveberg, M., Vuilleumier, S., and Fersht, A. R. (1994) Thermodynamic study of the acid denaturation of barnase and its dependence on ionic strength: Evidence for residual electrostatic interactions in the acid/thermally denatured state. *Biochemistry 33*, 8826–8832.
54. Trefethen, J. M., Pace, C. N., Scholtz, J. M., and Brems, D. N. (2005) Charge-charge interactions in the denatured state influence the folding kinetics of ribonuclease Sa. *Protein Sci. 14*, 1934–1938.
55. Sinha, K. K., and Udgaonkar, J. B. (2005) Dependence of the size of the initially collapsed form during the refolding of barstar on denaturant concentration: Evidence for a continuous transition. *J. Mol. Biol. 353*, 704–718.
56. Saxena, A. M., Udgaonkar, J. B., and Krishnamoorthy, G. (2006) Characterization of intra-molecular distances and site-specific dynamics in chemically unfolded barstar: Evidence for denaturant-dependent non-random structure. *J. Mol. Biol. 359*, 174–189.
57. Segel, D. J., Fink, A. L., Hodgson, K. O., and Doniach, S. (1998) Protein denaturation: A small-angle X-ray scattering study of the ensemble of unfolded states of cytochrome *c*. *Biochemistry 37*, 12443–12451.